



---

1 **Van Allen Probes observation of plasmaspheric**  
2 **hiss modulated by injected energetic electrons**

3 Run Shi<sup>1</sup>, Wen Li<sup>1</sup>, Qianli Ma<sup>2,1</sup>, Seth G. Claudepierre<sup>3</sup>, Craig A. Kletzing<sup>4</sup>, William S.  
4 Kurth<sup>4</sup>, George B. Hospodarsky<sup>4</sup>, Harlan E. Spence<sup>5</sup>, Geoff D. Reeves<sup>6</sup>, Joseph F. Fennell<sup>3</sup>,  
5 J. Bernard. Blake<sup>3</sup>, Scott A. Thaller<sup>7</sup>, and John R. Wygant<sup>7</sup>

6

7 <sup>1</sup>Center for Space Physics, Boston University, Boston, Massachusetts, USA.

8 <sup>2</sup>Department of Atmospheric and Oceanic Sciences, University of California, Los Angeles,  
9 Los Angeles, California, USA.

10 <sup>3</sup>Space Science Department, The Aerospace Corporation, El Segundo, California, USA.

11 <sup>4</sup>Department of Physics and Astronomy, University of Iowa, Iowa City, Iowa, USA.

12 <sup>5</sup>Institute for the Study of Earth, Oceans, and Space, University of New Hampshire,  
13 Durham, New Hampshire, USA.

14 <sup>6</sup>Space Science and Applications Group, Los Alamos National Laboratory, Los Alamos,  
15 New Mexico, USA.

16 <sup>7</sup>School of Physics and Astronomy, University of Minnesota, Twin Cities, Minneapolis,  
17 Minnesota, USA.

18

19



20 Corresponding author:

21 Run Shi

22 Center for Space Physics, Boston University, Boston, Massachusetts, USA

23 runs@bu.edu

24

25 **Key points**

26 1. Clear evidence is provided for local amplification of plasmaspheric hiss by anisotropic

27 electron distributions

28 2. Hiss wave intensity variation is well correlated with injected electron flux modulation

29 3. The modulation of injected electrons is correlated with ULF wave fluctuations

30



---

## 31 Abstract

32 Plasmaspheric hiss was observed by Van Allen Probe B in association with energetic  
33 electron injections in the outer plasmasphere. The energy of injected electrons coincides  
34 with the minimum resonant energy calculated for the observed hiss wave frequency.  
35 Interestingly, the variations of hiss wave intensity, electron flux, and ULF wave intensity  
36 exhibit remarkable correlations, while plasma density is not correlated with any of these  
37 parameters. Our study provides direct evidence for the first time that the injected  
38 anisotropic electron population, which is modulated by ULF waves, modulates the hiss  
39 intensity in the outer plasmasphere. This also implies that plasmaspheric hiss observed by  
40 Van Allen Probe B in the outer plasmasphere ( $L > \sim 5.5$ ) is locally amplified. Meanwhile,  
41 Van Allen Probe A observed hiss emission at lower  $L$  shells ( $< 5$ ), which was not associated  
42 with electron injections but primarily modulated by the plasma density. The features  
43 observed by Van Allen Probe A suggest that the observed hiss deep inside the plasmasphere  
44 may have propagated from higher  $L$  shells.

45

## 46 1. Introduction

47 Plasmaspheric hiss plays an important role in the loss of energetic electrons within the  
48 plasmasphere and in high-density plumes [Lyons *et al.*, 1972; Lyons and Thorne, 1973;  
49 Albert, 2005; Summers *et al.*, 2008; Ni *et al.*, 2013; Breneman *et al.*, 2015; Li *et al.*, 2015a;  
50 Ma *et al.*, 2016]. However, the generation mechanisms of plasmaspheric hiss remain under  
51 active research. Three mechanisms have received the most attention to explain the



---

52 generation of plasmaspheric hiss, including in situ growth of waves [Thorne *et al.*, 1979;  
53 Church and Thorne, 1983], lightning generated whistlers [Green *et al.*, 2005], and whistler  
54 mode chorus waves as an “embryonic source” [Bortnik *et al.* 2008, 2009; Chen *et al.* 2012a,  
55 2012b]. Although wave power above 2–3 kHz from lightning-generated whistlers shows  
56 some correlation with hiss waves [Green *et al.*, 2005], the waves below 1 kHz, which  
57 contain the majority of hiss wave power, are independent of lightning flash rate [Meredith  
58 *et al.*, 2006]. The in situ growth of waves inside the plasmasphere was shown to be  
59 inadequate to account for the observational level (~20 dB) [Huang *et al.*, 1983]; in response,  
60 Church and Thorne [1983] suggested that an “embryonic source” is required to lead to the  
61 observed wave intensity. Recent studies based on ray tracing simulation [Bortnik *et al.*,  
62 2008] have demonstrated that chorus waves from the distant magnetosphere can propagate  
63 into the plasmasphere and act as an embryonic source for the hiss wave generation.  
64 Furthermore, ray tracing simulations [Chen *et al.*, 2012a] suggested that the majority of  
65 hiss formation is caused by chorus emission originating within  $\sim 3 R_E$  from the plasmopause.  
66 This model has successfully explained the observed frequency spectrum and spatial  
67 distribution of the observed hiss over the typical hiss frequency range from 100 Hz to  
68 several kHz. A number of observational studies [Bortnik *et al.*, 2009; Wang *et al.*, 2011;  
69 Meredith *et al.* 2013; Li *et al.*, 2015b] have shown good correlations between chorus and  
70 plasmaspheric hiss and suggested that chorus plays an important role in hiss wave  
71 intensification.



---

72 Van Allen Probes recently detected unusually low frequency hiss emissions with wave  
73 power extending well below 100 Hz [*Li et al.*, 2013]. The low frequency hiss was  
74 demonstrated to cause more efficient loss of high energy electrons (in particular, ~50 keV  
75 to 1 MeV) than normal hiss and changes the electron pitch angle distributions [*Ni et al.*,  
76 2014; *Li et al.*, 2015a]. Such low frequency hiss is unlikely to be a result of propagation of  
77 chorus waves from a more distant region because embryonic chorus waves at the same  
78 frequency [*Bortnik et al.*, 2008] would need to originate from unrealistically high  $L$  shells  
79 [*Li et al.*, 2015b]. Therefore, these low frequency hiss waves were suggested to be  
80 generated in the outer plasmasphere on the dayside through local amplification [*Li et al.*,  
81 2013; *Chen et al.*, 2014; *Shi et al.*, 2017].

82 Hiss intensity modulation is often driven by the variation of background plasma  
83 density either through local amplification or wave propagation [*Chen et al.*, 2012c], and  
84 the modulation of hiss by other factors may easily be suppressed by the effect of the plasma  
85 density. Therefore, observations showing direct correlation between hiss emission and  
86 electron flux are still very limited. In fact, energetic electrons (tens to hundreds of keV)  
87 can be modulated by Ultra Low Frequency (ULF) waves. A typical modulation is caused  
88 by drift-resonance [*Southwood and Kivelson*, 1981]. *Zong et al.* [2009] showed an  
89 interesting event of energetic electron modulation by shock induced ULF waves. More  
90 recently, *Claudepierre et al.* [2013] presented observations of electron drift resonance with  
91 the fundamental poloidal mode of ULF waves based on Van Allen Probes measurements.  
92 The energy dependence of the amplitude and phase of the electron flux modulations



---

93 provided strong evidence for such an interaction. The peak electron flux modulations  
94 occurred over 5-6 wave cycles at energies  $\sim 60$  keV. The drift-resonance between electrons  
95 and ULF waves has been extensively studied both theoretically and observationally based  
96 on Van Allen Probes data [*Dai et al.*, 2013; *Hao et al.*, 2014; *Chen et al.*, 2016; *Zhou et al.*,  
97 2015, 2016; *Li et al.*, 2017]. Such modulation of energetic electrons may modulate hiss  
98 emissions by varying the electron flux and anisotropy, which could potentially affect the  
99 local growth rates of hiss waves, but the observational evidence has not been reported yet.  
100 In this study, we report on a modulation of hiss wave intensity and injected electron flux  
101 by ULF waves observed by Van Allen Probe B near the dayside, providing clear evidence  
102 that the hiss emission was generated through local amplification in the outer plasmasphere.

103

## 104 **2. Data and Methodology**

105 The Van Allen Probes comprise two identical spacecraft (Probes A and B) in near-  
106 equatorial orbits with an altitude of  $\sim 600$  km at perigee and geocentric distance of  $\sim 5.8 R_E$   
107 at apogee [*Mauk et al.*, 2012]. The Electric and Magnetic Field Instrument Suite and  
108 Integrated Science (EMFISIS) suite on Van Allen Probes A and B includes a magnetometer  
109 and a Waves instrument [*Kletzing et al.*, 2013]. The DC magnetic field is measured by the  
110 magnetometer, and the survey mode of Waveform Receiver (WFR) provides the power  
111 spectral density from 10 Hz to 12 kHz at 6 s time resolution. Plasma density can be either  
112 calculated based on the upper hybrid resonance frequency extracted from the High  
113 Frequency Receiver (HFR) data [*Kurth et al.*, 2015] or be inferred from the spacecraft



---

114 potential measured by the Electric Field and Waves (EFW) instrument [*Wygant et al.*,  
115 2013]. We inferred plasma density profiles based on the measurements from both  
116 instruments in the present study to obtain accurate plasma density values with high time  
117 resolution. High resolution electron flux measurements over the energy range of ~30 keV  
118 to 4 MeV are provided by the Magnetic Electron Ion Spectrometer (MagEIS) instrument  
119 [*Blake et al.*, 2013; *Spence et al.*, 2013]. We used the level 3 MagEIS dataset which  
120 includes particle pitch angle distribution in this study to evaluate the electron distribution  
121 responsible for the hiss wave generation.

122

### 123 **3. Observational Results**

124 A hiss intensification event modulated by electron injection was observed by Van  
125 Allen Probe B during ~20-22 UT on 12 January 2014, as shown in Figure 1. The satellite  
126 was located on the dayside and remained inside the plasmasphere, indicated by the high  
127 plasma density (Figure 1f). The main power of the hiss emission (Figures 1b and 1c)  
128 resided below the lower hybrid resonance frequency (white dash-dotted line in Figure 1b)  
129 and 100 Hz (white dashed line in Figure 1c) and intensified following the increase in the  
130 AE index (Figure 1a). Figure 1e presents the magnitude of the background magnetic field.  
131 Both the spin averaged electron flux (Figure 1g) and electron anisotropy (Figure 1h) exhibit  
132 modulations with a period of about 6 minutes. The electron anisotropy is calculated based  
133 on *Chen et al.* [1999]. The black lines in Figures 1g and 1h show the calculated minimum  
134 electron resonant energy for the first-order cyclotron resonance with parallel-propagating



---

135 right-hand polarized waves at a frequency of 40 Hz (magenta line in Figure 1b). As shown  
136 in Figure 1g, the minimum resonant energy captures the main energy of injected electrons.  
137 Figure 1i shows the electron pitch angle distribution at 54 keV which exhibits a pronounced  
138 modulation. The vertical dashed lines present the minima of the electron fluxes at 54 keV.  
139 Figure 1d illustrates the convective linear growth rates for parallel-propagating whistler  
140 mode waves that were calculated using the electron distribution measured by MagEIS  
141 based on the equations of *Summers et al.* [2009]. The modulation of linear growth rate  
142 appears to correlate well with the observed hiss wave spectral intensity with a period of  
143 several minutes.

144 Changes in the background magnetic field, plasma density and the injected electron  
145 distribution (flux and anisotropy of resonant electrons) could potentially be responsible for  
146 the hiss wave growth. Since the variation of the background magnetic field is small ( $\sim 4$   
147 nT) compared to the median value ( $\sim 150$  nT), the effect of background magnetic field on  
148 the wave growth rate is likely to be insignificant compared to the effects of plasma density  
149 and electron injection. To distinguish the roles of these two effects in the local wave  
150 amplification, we compared the hiss wave amplitude with spin averaged electron flux and  
151 plasma density. The hiss wave amplitude integrated from 20 Hz to 1000 Hz is shown in  
152 Figure 2a. Figure 2b presents the spin averaged electron flux integrated over the energy  
153 range from 30 keV to 200 keV. The vertical dashed lines in Figure 2 depict the same times  
154 as in Figure 1.



---

155 Figure 2c shows the comparison between the filtered electron flux (black) over 1.5  
156 MHz - 4 MHz and the filtered hiss wave intensity (blue) over 1.5 MHz - 4 MHz. It suggests  
157 that the hiss intensity is well correlated with the variation of the electron flux. The  
158 correlation coefficient between the filtered electron flux and the filtered hiss wave intensity  
159 in the time period from 20:00 UT to 22:00 UT is 0.841. The satellite was located at a  
160 magnetic latitude of  $-1.3^{\circ}$ ~ $-2.0^{\circ}$ , which was near the source region where local wave  
161 amplification typically occurs, and this is probably why hiss intensity and electron flux  
162 exhibit a remarkable correlation.

163 In the present hiss modulation event, the filtered background plasma density (green  
164 line in Figure 2d) is not well correlated with the filtered wave intensity (with a correlation  
165 coefficient of 0.105), especially during the period from 20:45 UT to 21:40 UT. This  
166 suggests that the variation of plasma density plays an insignificant role in the modulation  
167 of hiss wave intensity during this event. To investigate the sole effect of density on hiss  
168 intensity, we also calculated the correlation coefficient between the non-filtered hiss wave  
169 intensity and non-filtered the plasma density which even shows a slight anti-correlation  
170 with a coefficient of  $\sim -0.483$ .

171 The electron flux variation observed by Van Allen Probe B may be caused by ULF  
172 wave modulation since they have similar time periods. Figure 3 shows the variation of  
173 electron fluxes at different energy channels observed by both Van Allen Probe A (a) and  
174 Van Allen Probe B (b). At  $\sim 19:30$ UT, both probes, especially Van Allen Probe B observed  
175 intense electron injections. Between 20:00 and 22:00 UT, the energetic electrons observed



---

176 by Probe B are modulated at most energy channels, with a time period of several minutes  
177 in the same frequency range as typical ULF waves (Pc4-5).

178 Figure 4 is the summary of the Pc4-5 ULF waves from Van Allen Probe B during the  
179 time interval of interest (20:00–22:00 UT). Dynamic spectrograms of the ULF wave  
180 powers are shown for the three components of the magnetic field (in the mean field-aligned,  
181 geocentric solar magnetospheric (GSM) coordinates) along with the  $y$  component of the  
182 electric field in modified geocentric solar elliptic (MGSE) coordinate. Band-pass filtered  
183 time series (1.5–4 mHz) are shown below for each dynamic spectrogram. The parallel  
184 magnetic field ( $B_{\text{para}}$ ) and  $y$  component electric field in MGSE coordinate ( $E_y$ ) have a  
185 similar frequency peak at  $\sim 2.6$  mHz. The wave spectra of the  $E_y$  and  $B_{\text{para}}$  components  
186 suggest that the compressional mode and shear mode are likely coupled.

187 The correlation of the ULF waves and the energetic electron fluxes at different energy  
188 channels is shown in Figure 5. Figure 5a illustrates the filtered  $E_y$  component of the electric  
189 field between 1.5 and 4 mHz. Since Van Allen Probe B is near noon, the  $E_y$  component  
190 approximately represents the electric field in the azimuthal direction. Band-pass filtered  
191 electron fluxes normalized by unperturbed levels at different energy channels are shown in  
192 Figure 5b. The vertical black lines indicate the minima of the  $E_y$  component. The electron  
193 fluxes at various energies show a modulation period which is very similar to that of  $E_y$ .  
194 Besides, these fluxes exhibit an energy-dependent phase shift with respect to  $E_y$ . The phase  
195 of the electron flux oscillations with respect to  $E_y$  is closest to  $180^\circ$  out-of-phase at  $\sim 466$   
196 keV. At lower energies, the phase of peak electron fluxes relative to the  $E_y$  minimum varies



---

197 but is not  $180^\circ$  out-of-phase. For the observed modulating hiss, the minimum resonant  
198 energy is tens of keV (Figure 1), and thus the electron flux at energy below 100 keV plays  
199 a dominant role in hiss amplification. Although these low energy electrons (30–100 keV)  
200 are not exactly in drift resonance with the observed ULF waves, their modulation is highly  
201 relevant to the presence of ULF waves.

202 Meanwhile, Van Allen Probe A detected hiss emissions in a similar frequency range  
203 as shown in Figure 6. During this time period, Van Allen Probe A was located at lower  $L$   
204 shells ( $2.6 < L < 5.3$ ) and later MLTs ( $14.9 < \text{MLT} < 18.0$ ). The hiss intensity also exhibited  
205 modulation in electric and magnetic field, as shown in Figures 6b and 6c, respectively.  
206 However, different from the observation by Probe B, the hiss intensity is dominantly  
207 modulated by the variation of the plasma density. Figure 6d shows the density profile  
208 obtained from EMFISIS (black) and EFW (red). Examples of evident modulations by  
209 variation of plasma density are highlighted with grey blocks. According to ray tracing  
210 simulation [*Chen et al.*, 2012c], the hiss waves tend to propagate to the region with higher  
211 density resulting in higher wave intensity. Figures 6e and 6f show the spin averaged  
212 electron flux and anisotropy based on MagEIS data and the white lines are the minimum  
213 resonant energy corresponding to a frequency of 40 Hz (Figure 6b). There is no clear  
214 correlation between the hiss intensity and electron flux, suggesting that the modulations  
215 are mainly caused by the plasma density variation. We also calculated the convective linear  
216 growth rates for parallel-propagating whistler mode waves as shown in Figure 6g. The



---

217 growth rate profile shows little correlation with that of the observed hiss intensity,  
218 indicating that these waves are not locally excited.

219 Figure 7 illustrates the comparison of hiss wave frequency spectra observed by Van  
220 Allen Probes A (Figures 7a-7b) and B (Figures 7c-7d). At the beginning of the emission  
221 around 20:20 UT, the hiss wave intensity as a function of frequency observed by Van Allen  
222 Probe A presents a minimum at ~200 Hz (indicated by the white arrows in Figures 7a and  
223 7b). This feature is similar to the observation by Van Allen Probe B (Figures 7c and 7d),  
224 where the modulation of hiss wave power below 100 Hz is correlated with the calculated  
225 wave growth rate (Figure 1d) based on the observed electron distribution. The hiss wave  
226 frequency spectra and structures observed by Probe A are similar to those observed by  
227 Probe B, but the energy spectra of energetic electrons are significantly different. Therefore,  
228 the hiss emission observed by Probe A may be the result of wave propagation from the  
229 source region in the outer plasmasphere and further modulated by the local plasma density  
230 variation.

231

#### 232 **4. Summary and Discussion**

233 We report clear evidence of local amplification of plasmaspheric hiss observed by Van  
234 Allen Probe B in the postnoon sector of the outer plasmapshere. The minimum resonance  
235 energy calculated for the observed hiss wave frequency is consistent with the energy of  
236 injected electrons. The hiss wave intensity was modulated by the injected energetic  
237 electrons, which were modulated by ULF waves. In the meantime, Van Allen Probe A also



---

238 observed similar hiss emissions at lower  $L$  shells, which is probably due to the propagation  
239 from the source region in the outer plasmasphere. Different from the observation by Probe  
240 B, the hiss wave intensity observed by Probe A is predominantly affected by the  
241 background plasma density. The modulation of hiss intensity by plasma density could be  
242 due to the effect of ray focusing at high-density region during propagation [*Chen et al.*,  
243 2012c].

244 Figure 8 summarizes the processes discussed in this study. The injected energetic  
245 electrons with energies of tens to hundreds of keV drift from the nightside to the dayside  
246 in the outer plasmasphere. Simultaneously, the ULF waves modulate the energetic electron  
247 fluxes. The modulated energetic electrons then lead to the modulation of the hiss intensity  
248 via local amplification. These features were all well captured by Van Allen Probe B. During  
249 the same time period, Probe A at a later MLT and lower  $L$  shell observed hiss emissions  
250 which may originate from the source region in the outer plasmasphere.

251 Chorus waves which are intense coherent electromagnetic emissions exhibiting discrete  
252 rising or falling tones are believed to be generated through cyclotron resonance with  
253 anisotropic electrons [*Kennel and Petschek*, 1966; *Anderson and Maeda*, 1977; *Meredith*  
254 *et al.*, 2001; *Li et al.*, 2009]. It has been shown that ULF waves can modulate chorus  
255 intensity by modulating the background magnetic field and/or plasma density which affect  
256 the number of energetic electrons resonant with chorus waves [*Li et al.*, 2011]. Besides, the  
257 ULF wave-induced modulation of chorus could have an impact on electron precipitation  
258 leading to pulsating aurora [*Jaynes et al.*, 2015]. Similar modulations may also be captured



---

259 in hiss wave intensity if hiss is locally amplified. However, different from chorus,  
260 plasmaspheric hiss waves are commonly known to be structureless [*Thorne et al.*, 1973]  
261 and wave propagation is believed to be important for the measured hiss wave  
262 intensification [*Bortnik et al.*, 2008, 2009; *Chen et al.*, 2014]. The hiss wave intensity is  
263 typically modulated by the variation of the background plasma density [*Chen et al.*, 2012c].  
264 Nonetheless, our study showed the first evidence of the hiss wave modulation caused by  
265 modulated injected electrons due to ULF waves, clearly indicating that the hiss is locally  
266 amplified in the outer plasmasphere. It also provides an interesting link between the ULF  
267 waves and hiss waves which are in two distinct frequency ranges but both play important  
268 roles in radiation belt electron dynamics.

269

## 270 **Acknowledgments**

271 The work at Boston University is supported by the NASA grants NNX15AI96G,  
272 NNX17AG07G, and NNX17AD15G and NSF grant AGS-1723342. The research at the  
273 University of Minnesota was supported by JHU/APL contract UMN 922613 under NASA  
274 contract JHU/APL NAS5-01072. We acknowledge the RBSP-ECT and EMFISIS funding  
275 provided by JHU/APL contract No. 967399 and 921647 under NASA's prime contract No.  
276 NAS5-01072. We would like to thank Dr. Lei Dai and Dr. Xu-Zhi Zhou for very helpful  
277 discussions in this study. We would like to acknowledge the EMFISIS data obtained from  
278 <http://emfisis.physics.uiowa.edu>, the MagEIS data obtained from [http://www.rbbsp-](http://www.rbbsp-ect.lanl.gov/science/DataDirectories.php)  
279 [ect.lanl.gov/science/DataDirectories.php](http://www.rbbsp-ect.lanl.gov/science/DataDirectories.php), and the EFW data obtained from



---

280 <http://rbsp.space.umn.edu/data/rbsp/>. We also thank the World Data Center for  
281 Geomagnetism, Kyoto for providing AE index used in this study.



---

## 282 **References**

- 283 Albert, J. M. (2005), Evaluation of quasi-linear diffusion coefficients for whistler mode  
284 waves in a plasma with arbitrary density ratio, *J. Geophys. Res.*, *110*, A03218,  
285 doi:10.1029/2004JA010844.
- 286 Anderson, R. R., and K. Maeda (1977), VLF emissions associated with enhanced  
287 magnetospheric electrons, *J. Geophys. Res.*, *82*(1), 135–146,  
288 doi:10.1029/JA082i001p00135.
- 289 Blake, J. B., et al. (2013), The Magnetic Electron Ion Spectrometer (MagEIS) Instruments  
290 Aboard the Radiation Belt Storm Probes (RBSP) spacecraft, *Space. Sci. Rev.*,  
291 doi:10.1007/s11214-013-9991-8.
- 292 Bortnik, J., R. M. Thorne, and N. P. Meredith (2008), The unexpected origin of  
293 plasmaspheric hiss from discrete chorus emissions, *Nature*, *452*, 62–66,  
294 doi:10.1038/nature06741.
- 295 Bortnik, J., W. Li, R. M. Thorne, V. Angelopoulos, C. Cully, J. Bonnell, O. Le Contel, and  
296 A. Roux (2009), An Observation linking the origin of plasmaspheric hiss to discrete  
297 chorus emissions, *Science*, *324*, 775–778, doi:10.1126/science.1171273.
- 298 Breneman, A. W., et al. (2015), Global-scale coherence modulation of radiation-belt  
299 electron loss from plasmaspheric hiss, *Nature*, *523*, 193–195, doi:10.1038/nature14515.
- 300 Chen, M. W., J. L. Roeder, J. F. Fennell, L. R. Lyons, R. L. Lambour, and M. Schulz (1999),  
301 Proton ring current pitch angle distributions: Comparison of simulations with CRRES  
302 observations, *J. Geophys. Res.*, *104*(A8), 17,379–17,389.



- 
- 303 Chen, L., J. Bortnik, W. Li, R. M. Thorne, and R. B. Horne (2012a), Modeling the  
304 properties of plasmaspheric hiss: 1. Dependence on chorus wave emission, *J. Geophys.*  
305 *Res.*, *117*, A05201, doi:10.1029/2011JA017201.
- 306 Chen, L., J. Bortnik, W. Li, R.M. Thorne, and R. B. Horne (2012b), Modeling the  
307 properties of plasmaspheric hiss: 2. Dependence on the plasma density distribution, *J.*  
308 *Geophys. Res.*, *117*, A05202, doi:10.1029/2011JA017202.
- 309 Chen, L., R. M. Thorne, W. Li, J. Bortnik, D. Turner, and V. Angelopoulos (2012c),  
310 Modulation of plasmaspheric hiss intensity by thermal plasma density structure,  
311 *Geophys. Res. Lett.*, *39*, L14103, doi:10.1029/2012GL052308.
- 312 Chen, L., et al. (2014), Generation of unusually low frequency plasmaspheric hiss, *Geophys.*  
313 *Res. Lett.*, *41*, 5702–5709, doi:10.1002/2014GL060628.
- 314 Chen, X.-R., Q.-G. Zong, X.-Z. Zhou, J. B. Blake, J. R. Wygant, and C. A.  
315 Kletzing (2016), Van allen probes observation of a 360° phase shift in the flux  
316 modulation of injected electrons by ULF waves, *Geophys. Res. Lett.*, *44*, 1614–1624,  
317 doi:10.1002/2016GL071252.
- 318 Church, S. R., and R. M. Thorne (1983), On the origin of plasmaspheric hiss—Raypath  
319 integrated amplification, *J. Geophys. Res.*, *88*, 7941–7957,  
320 doi:10.1029/JA088iA10p07941.
- 321 Huang, C. Y., C. K. Goertz, and R. R. Anderson (1983), A theoretical study of plasmaspheric  
322 hiss generation, *J. Geophys. Res.*, *88*, 7927–7940, doi:10.1029/JA088iA10p07927.



- 
- 323 Claudepierre, S. G., et al. (2013), Van Allen Probes observation of localized drift resonance  
324 between poloidal mode ultra-low frequency waves and 60 keV electrons, *Geophys. Res.*  
325 *Lett.*, *40*, 4491–4497, doi:10.1002/grl.50901.
- 326 Dai, L., et al. (2013), Excitation of poloidal standing Alfvén waves through drift resonance  
327 wave-particle interaction, *Geophys. Res. Lett.*, *40*, 4127–4132, doi:10.1002/grl.50800.
- 328 Green, J. L., S. Boardsen, L. Garcia, W. W. L. Taylor, S. F. Fung, and B. W. Reinisch  
329 (2005), On the origin of whistler mode radiation in the plasmasphere, *J. Geophys. Res.*,  
330 *110*, A03201, doi:10.1029/2004JA010495.
- 331 Hao, Y. X., et al. (2014), Interactions of energetic electrons with ULF waves triggered by  
332 interplanetary shock: Van Allen Probes observations in the magnetotail, *J. Geophys.*  
333 *Res. Space Physics*, *119*, 8262–8273, doi:10.1002/2014JA020023.
- 334 Jaynes, A. N., et al. (2015), Correlated Pc4–5 ULF waves, whistler-mode chorus, and  
335 pulsating aurora observed by the Van Allen Probes and ground-based systems, *J.*  
336 *Geophys. Res. Space Physics*, *120*, 8749–8761, doi:10.1002/2015JA021380.
- 337 Kennel, C. F., and H. E. Petschek (1966), Limit on stably trapped particle fluxes, *J.*  
338 *Geophys. Res.*, *71*(1), 1–28, doi:10.1029/JZ071i001p00001.
- 339 Kletzing, C. A., et al. (2013), The Electric and Magnetic Field Instrument Suite and  
340 Integrated Science (EMFISIS) on RBSP, *Space Sci. Rev.*, *179*, 127–181,  
341 doi:10.1007/s11214-013-9993-6.
- 342 Kurth, W. S., De Pascuale, S., Faden, J. B., Kletzing, C. A., Hospodarsky, G. B., Thaller,  
343 S. and Wygant, J. R. (2015), Electron densities inferred from plasma wave spectra



- 
- 344 obtained by the Waves instrument on Van Allen Probes. *J. Geophys. Res. Space*  
345 *Physics*, 120: 904–914. doi: 10.1002/2014JA020857.
- 346 Li, L., X.-Z. Zhou, Q.-G. Zong, R. Rankin, H. Zou, Y. Liu, X.-R. Chen, and Y.-X.  
347 Hao (2017), Charged particle behavior in localized ultralow frequency waves: Theory  
348 and observations, *Geophys. Res. Lett.*, 44, 5900–5908, doi:10.1002/2017GL073392.
- 349 Li, W., R. M. Thorne, V. Angelopoulos, J. W. Bonnell, J. P. McFadden, C. W. Carlson, O.  
350 LeContel, A. Roux, K. H. Glassmeier, and H. U. Auster (2009), Evaluation of whistler-  
351 mode chorus intensification on the nightside during an injection event observed on the  
352 THEMIS spacecraft, *J. Geophys. Res.*, 114, A00C14, doi:10.1029/2008JA013554.
- 353 Li, W., R. M. Thorne, J. Bortnik, Y. Nishimura, and V. Angelopoulos (2011), Modulation  
354 of whistler mode chorus waves: 1. Role of compressional Pc4–5 pulsations, *J. Geophys.*  
355 *Res.*, 116, A06205, doi:10.1029/2010JA016312.
- 356 Li, W., et al. (2013), An unusual enhancement of low-frequency plasmaspheric hiss in the  
357 outer plasmasphere associated with substorm-injected electrons, *Geophys. Res. Lett.*,  
358 40, 3798–3803, doi:10.1002/grl.50787.
- 359 Li, W., Q. Ma, R. M. Thorne, J. Bortnik, C. A. Kletzing, W. S. Kurth, G. B. Hospodarsky,  
360 and Y. Nishimura (2015a), Statistical properties of plasmaspheric hiss derived from  
361 Van Allen Probes data and their effects on radiation belt electron dynamics. *J. Geophys.*  
362 *Res. Space Physics*, 120, 3393–3405. doi: 10.1002/2015JA021048.
- 363 Li, W., L. Chen, J. Bortnik, R. M. Thorne, V. Angelopoulos, C. A. Kletzing, W. S. Kurth,  
364 and G. B. Hospodarsky (2015b), First evidence for chorus at a large geocentric distance



- 
- 365 as a source of plasmaspheric hiss: Coordinated THEMIS and Van Allen Probes  
366 observation, *Geophys. Res. Lett.*, 42, 241–248, doi:10.1002/2014GL062832.
- 367 Lyons, L. R., R. M. Thorne, and C. F. Kennel (1972), Pitch-angle diffusion of radiation  
368 belt electrons within the plasmasphere, *J. Geophys. Res.*, 77(19), 3455–3474,  
369 doi:10.1029/JA077i019p03455.
- 370 Lyons, L. R., and R. M. Thorne (1973), Equilibrium structure of radiation belt electrons, *J.*  
371 *Geophys. Res.*, 78(13), 2142–2149, doi:10.1029/JA078i013p02142.
- 372 Ma, Q., et al. (2016), Characteristic energy range of electron scattering due to  
373 plasmaspheric hiss, *J. Geophys. Res. Space Physics*, 121, 11,737–11,749,  
374 doi:10.1002/2016JA023311.
- 375 Mauk, B. H., N. J. Fox, S. G. Kanekal, R. L. Kessel, D. G. Sibeck, and A. Ukhorskiy (2012),  
376 Science Objectives and Rationale for the Radiation Belt Storm Probes Mission, *Space*  
377 *Sci. Rev.*, 1–15, doi:10.1007/s11214-012-9908-y.
- 378 Meredith, N. P., R. B. Horne, and R. R. Anderson (2001), Substorm dependence of chorus  
379 amplitudes: Implications for the acceleration of electrons to relativistic energies, *J.*  
380 *Geophys. Res.*, 106(A7), 13,165–13,178, doi:10.1029/2000JA900156.
- 381 Meredith, N. P., R. B. Horne, M. A. Clilverd, D. Horsfall, R. M. Thorne, and R. R.  
382 Anderson (2006), Origins of plasmaspheric hiss, *J. Geophys. Res.*, 111, A09217,  
383 doi:10.1029/2006JA011707.



- 
- 384 Meredith, N. P., R. B. Horne, J. Bortnik, R. M. Thorne, L. Chen, W. Li, and A. Sicard-  
385 Piet (2013), Global statistical evidence for chorus as the embryonic source of  
386 plasmaspheric hiss, *Geophys. Res. Lett.*, *40*, 2891-2896, doi:10.1002/grl.50593.
- 387 Ni, B., J. Bortnik, R. M. Thorne, Q. Ma, and L. Chen (2013), Resonant scattering and  
388 resultant pitch angle evolution of relativistic electrons by plasmaspheric hiss, *J.*  
389 *Geophys. Res. Space Physics*, *118*, 7740–7751, doi:10.1002/2013JA019260.
- 390 Ni, B., et al. (2014), Resonant scattering of energetic electrons by unusual low-frequency  
391 hiss, *Geophys. Res. Lett.*, *40*, 3798–3803, doi:10.1002/grl.50787.
- 392 Shi, R., Li, W., Ma, Q., Reeves, G. D., Kletzing, C. A., Kurth, W. S., ... Claudepierre, S.  
393 G. (2017). Systematic evaluation of low-frequency hiss and energetic electron  
394 injections. *Journal of Geophysical Research: Space Physics*, *122*, 10,263–  
395 10,274. <https://doi.org/10.1002/2017JA024571>.
- 396 Southwood, D. J., and M. G. Kivelson (1981), Charged particle behavior in low-frequency  
397 geomagnetic pulsations. I Transverse waves, *J. Geophys. Res.*, *86*, 5643–5655,  
398 doi:10.1029/JA086iA07p05643.
- 399 Spence, H. E., et al. (2013), Science Goals and Overview of the Energetic Particle,  
400 Composition, and Thermal Plasma (ECT) Suite on NASA's Radiation Belt Storm  
401 Probes (RBSP) Mission, *Space Sci. Rev.*, doi:10.1007/s11214-013-0007-5.
- 402 Summers, D., B. Ni, N. P. Meredith, R. B. Horne, R. M. Thorne, M. B. Moldwin, and R.  
403 R. Anderson (2008), Electron scattering by whistler-mode ELF hiss in plasmaspheric  
404 plumes, *J. Geophys. Res.*, *113*, A04219, doi:10.1029/2007JA012678.



- 
- 405 Summers, D., R. Tang, and R. M. Thorne (2009), Limit on stably trapped particle fluxes in  
406 planetary magnetospheres, *J. Geophys. Res.*, *114*, A10210, doi:10.1029/2009JA014428.
- 407 Thorne, R. M., E. J. Smith, R. K. Burton, and R. E. Holzer (1973), Plasmaspheric hiss, *J.*  
408 *Geophys. Res.*, *78*(10), 1581–1596, doi:10.1029/JA078i010p01581.
- 409 Thorne, R. M., S. R. Church, and D. J. Gorney (1979), On the origin of plasmaspheric  
410 hiss—The importance of wave propagation and the plasmopause, *J. Geophys. Res.*, *84*,  
411 5241–5247, doi:10.1029/JA084iA09p05241.
- 412 Wang, C., Q. Zong, F. Xiao, Z. Su, Y. Wang, and C. Yue (2011), The relations between  
413 magnetospheric chorus and hiss inside and outside the plasmasphere boundary layer:  
414 Cluster observation, *J. Geophys. Res.*, *116*, A07221, doi:10.1029/2010JA016240.
- 415 Wygant J. R. et al. (2013), The Electric Field and Waves Instruments on the Radiation Belt  
416 Storm Probes Mission, *Space Science Reviews*, *179*, (1-4), pp.183-220,  
417 doi: 10.1007/s11214-013-0013-7.
- 418 Zhou, X.-Z., Z.-H. Wang, Q.-G. Zong, S. G. Claudepierre, I. R. Mann, M. G. Kivelson, V.  
419 Angelopoulos, Y.-X. Hao, Y.-F. Wang, and Z.-Y. Pu (2015), Imprints of impulse-  
420 excited hydromagnetic waves on electrons in the Van Allen radiation belts, *Geophys.*  
421 *Res. Lett.*, *42*, 6199–6204, doi:10.1002/2015GL064988.
- 422 Zhou, X.-Z., Z.-H. Wang, Q.-G. Zong, R. Rankin, M. G. Kivelson, X.-R. Chen, J. B.  
423 Blake, J. R. Wygant, and C. A. Kletzing (2016), Charged particle behavior in the  
424 growth and damping stages of ultralow frequency waves: Theory and Van Allen Probes



---

425 observations, *J. Geophys. Res. Space Physics*, *121*, 3254–3263,

426 doi:10.1002/2016JA022447.

427 Zong, Q.-G., et al. (2009), Energetic electron response to ULF waves induced by

428 interplanetary shocks in the outer radiation belt, *J. Geophys. Res.*, *114*, A10204,

429 doi:10.1029/2009JA014393.



---

## 430 **Figure Captions**

431 **Figure 1.** Plasmaspheric hiss modulation caused by injected electrons observed by Van  
432 Allen Probe B from 20:00 UT to 22:00 UT on January 12, 2014. (a) *AE* index; frequency-  
433 time spectrogram of (b) wave electric field and (c) wave magnetic field spectral density in  
434 the WFR channel; (d) frequency spectrum of convective linear wave growth rates; (e)  
435 background magnetic field intensity; (f) calibrated plasma density based on EFW and  
436 EMFISIS; (g) spin-averaged electron flux measured by MagEIS; (h) electron anisotropy;  
437 (i) pitch angle distribution of electrons at 54 keV. The white dash-dotted line in Figure 1b  
438 represents the lower hybrid resonance frequency ( $f_{LHR}$ ). The magenta line in Figure 1b  
439 indicates 40 Hz. The white dashed line in Figure 1c indicates 100 Hz. The black lines in  
440 Figures 1g and 1h represent the minimum resonant energy of electrons interacting with the  
441 waves at 40 Hz. The dashed vertical lines mark the modulation of the electron flux at 54  
442 keV (Figure 1i).

443 **Figure 2.** (a) Integrated hiss intensity from 20 Hz to 1000 Hz; (b) integrated spin-averaged  
444 electron flux from 30 keV to 200 keV; (c) filtered integrated electron number flux (black)  
445 and filtered magnetic wave intensity of hiss (blue); (d) filtered plasma density (green) and  
446 filtered magnetic wave intensity of hiss (blue). The vertical dashed lines depict the same  
447 times as those in Figure 1.

448 **Figure 3.** Variation of electron fluxes at different energies observed by Van Allen Probe  
449 A (a) and Van Allen Probe B (b). In Figure 3b, the modulation of electron fluxes was



---

450 observed by Van Allen Probe B between 20:00:00 and 22:00:00 UT in association with  
451 ULF waves, and the dispersed electron injection was observed at ~19:30:00 UT.

452 **Figure 4.** Summary of the Pc4-5 ULF wave frequency spectra from Van Allen Probe B  
453 during the time interval of interest (20:00-22:00 UT). Dynamic spectrograms are shown  
454 for the three components of the magnetic field (in the mean field-aligned, GSM coordinates)  
455 along with the  $y$  component of the electric field in MGSE coordinate. Band-pass filtered  
456 time series (1.5 - 4 mHz) are shown below for each dynamic spectrogram. The black dashed  
457 lines indicate the frequency at ~2.6 mHz.

458 **Figure 5.** The correlation of the filtered (1.5 - 4 mHz)  $E_y$  component of ULF waves (a) and  
459 the energetic electron fluxes at different energy channels (b). The electron fluxes show the  
460 modulation in the similar period to that of  $E_y$ , but exhibit an energy-dependent phase shift  
461 with respect to  $E_y$ .

462 **Figure 6.** The observation of waves and electron fluxes by Van Allen Probe A during the  
463 same period as that in Figure 1. a)  $AE$  index; (b) frequency-time spectrogram of wave  
464 electric field and (c) wave magnetic spectral density in the WFR channel; (d) plasma  
465 density obtained by EFW (red) and EMFISIS (black); (e) spin-averaged electron flux  
466 measured by MagEIS; (f) electron anisotropy; (g) convective wave growth rates. Grey  
467 block areas indicate the intervals of hiss modulation by variation of plasma density. The  
468 magenta line in Figure 6b indicates 40 Hz. The black dashed line in Figure 6c indicates 100  
469 Hz. The white lines in Figures 6e and 6f represent the minimum resonant energy of  
470 electrons for the waves at 40 Hz.



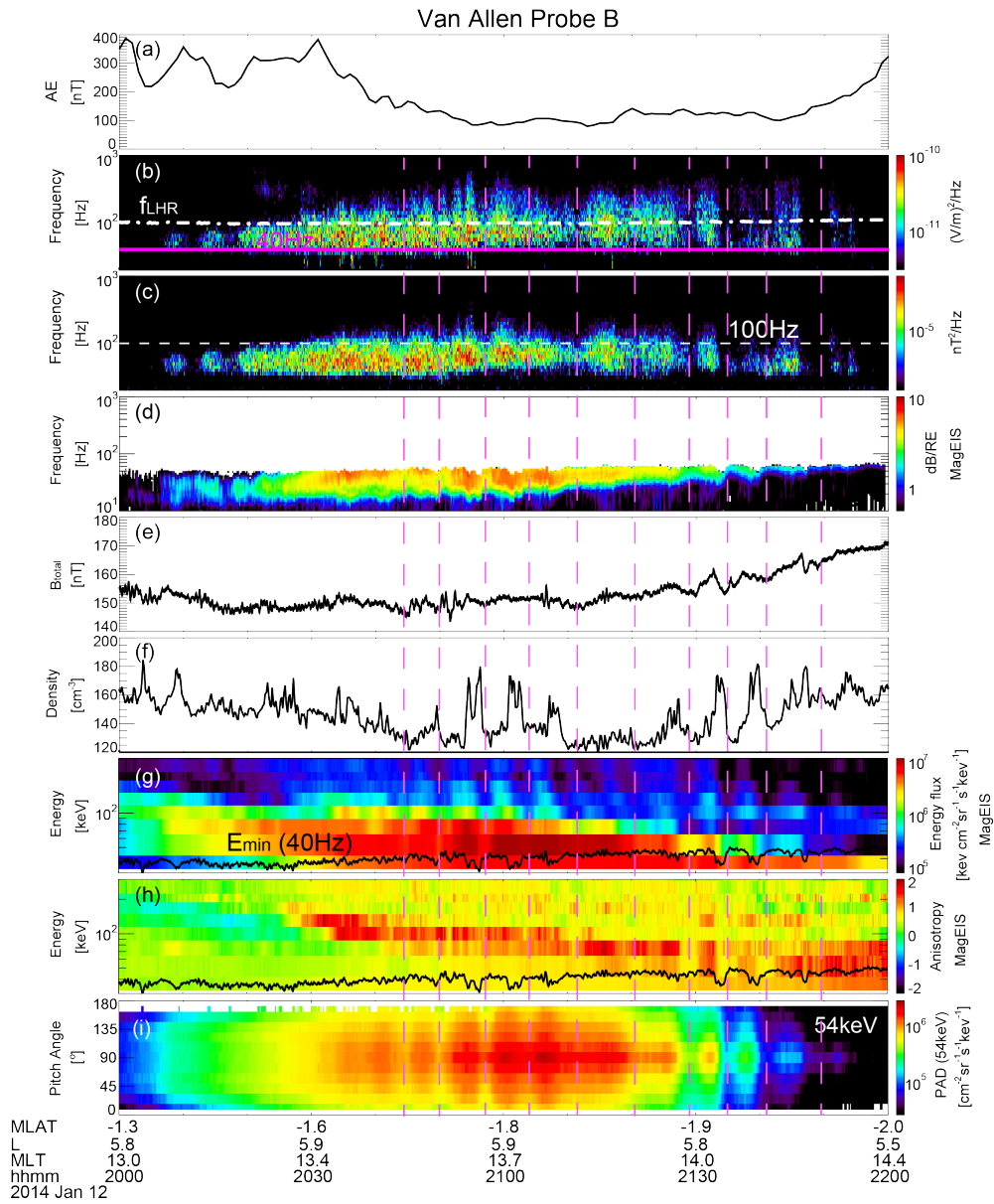
---

471 **Figure 7.** The wave electric (a) and magnetic (b) spectral density observed by Van Allen  
472 Probe A and the wave electric (c) and magnetic (d) spectral density from Van Allen Probe  
473 B. Note that at the beginning of the emissions around 20:20 UT, the hiss wave intensity as  
474 a function of frequency presents a minimum at ~200 Hz (white arrows) for the observations  
475 from both Van Allen Probes A and B.

476 **Figure 8.** A cartoon showing energetic electron trajectory (green), ULF waves (pink) and  
477 hiss intensity modulation (blue). Injected electrons from the nightside drift to the postnoon  
478 sector (green arrow) in the outer plasmasphere where they provide a source of free energy  
479 for hiss wave generation in the outer plasmasphere. During the period of electron injection,  
480 electrons are modulated by ULF waves (magenta), which lead to the modulation of hiss  
481 wave amplification (blue), as observed by Van Allen Probe B. The hiss waves are probably  
482 generated in the outer plasmasphere, and then propagate into lower  $L$  shells, as observed  
483 by Van Allen Probe A.

484

485 Figure 1

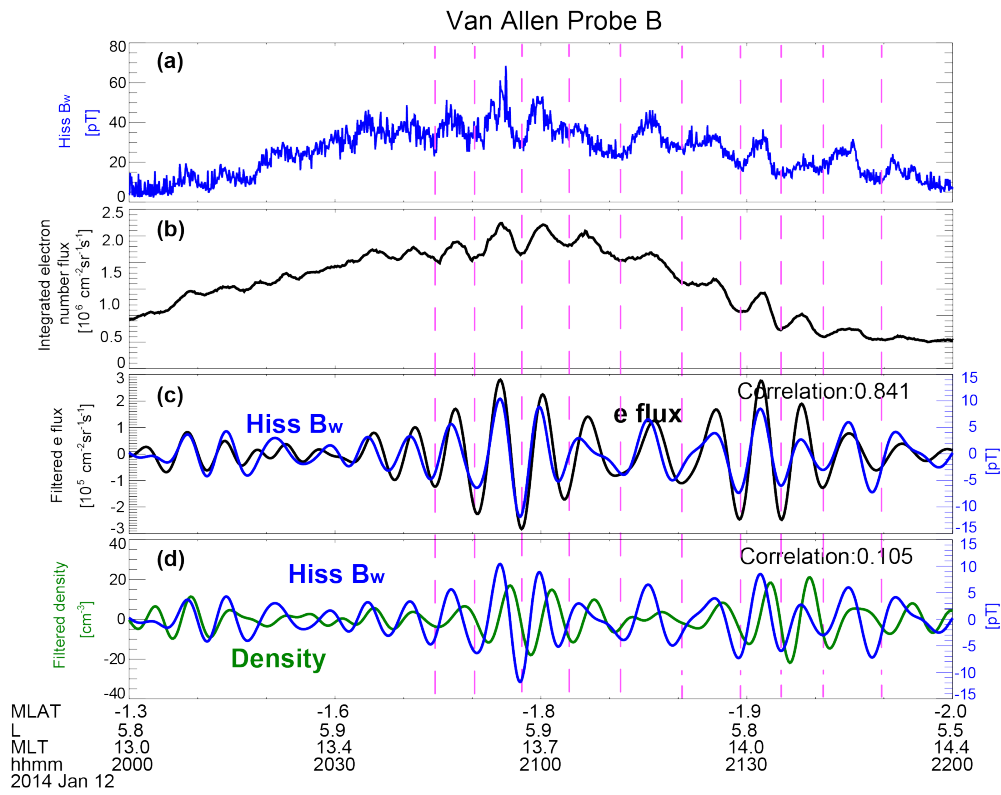


486

487

488 Figure 2

489



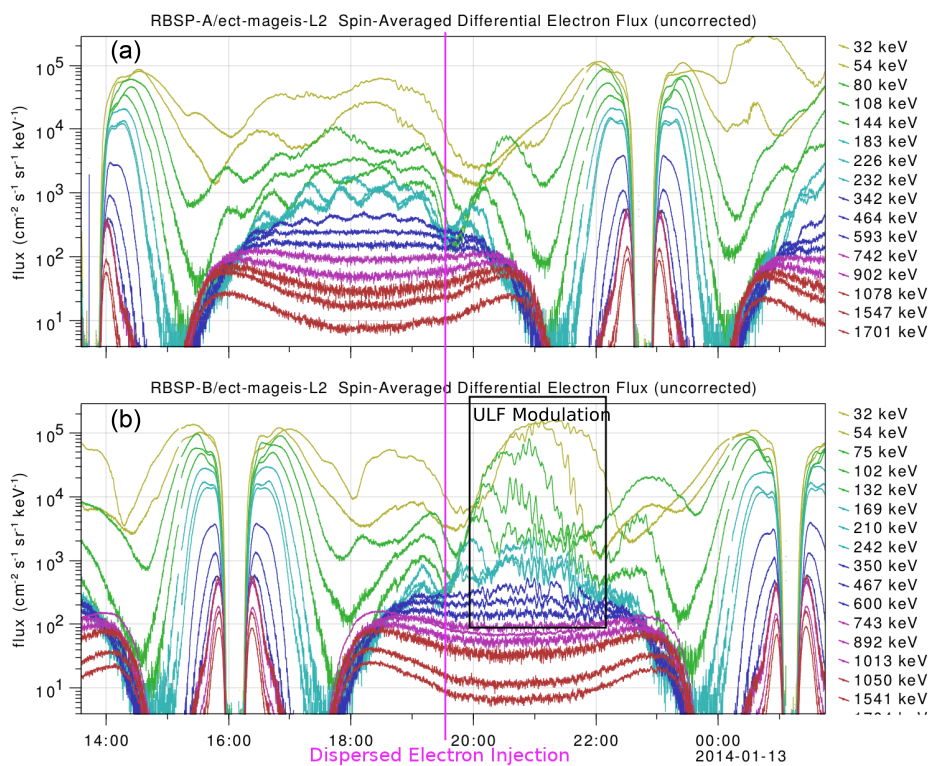
490

491

492



493 Figure 3.



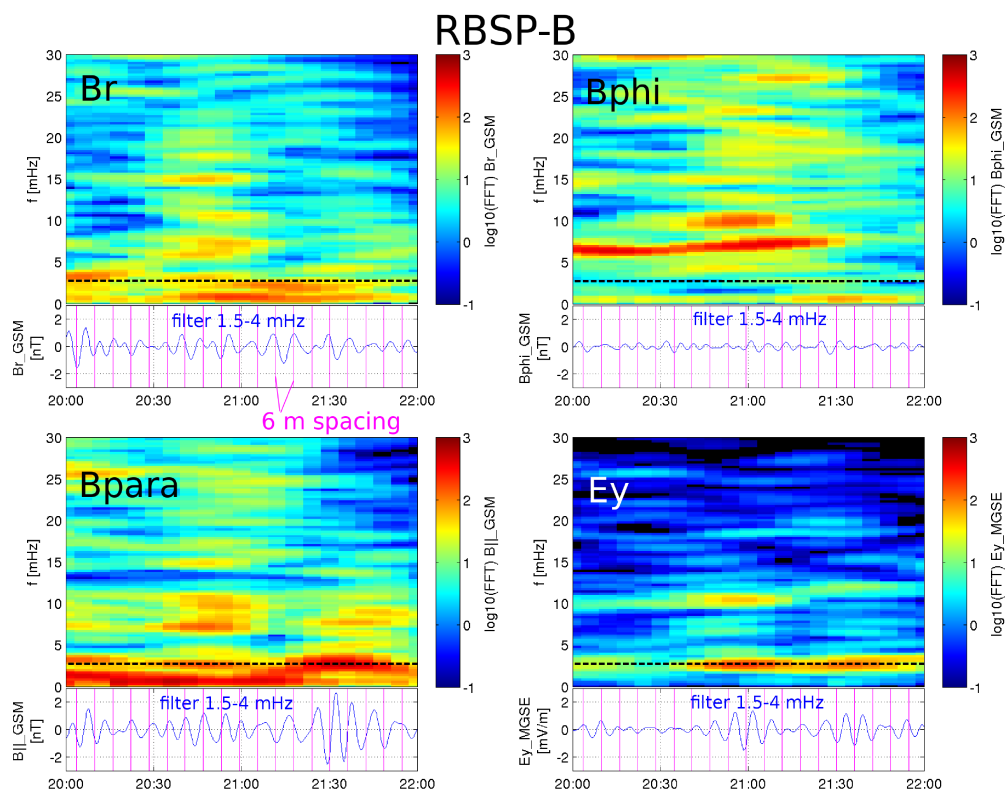
494

495

496



497 Figure 4

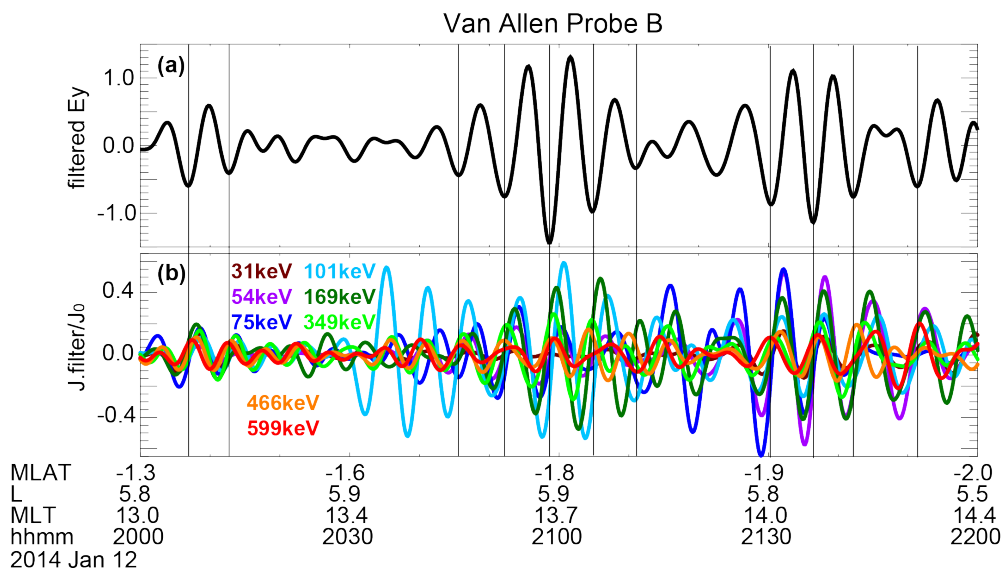


498

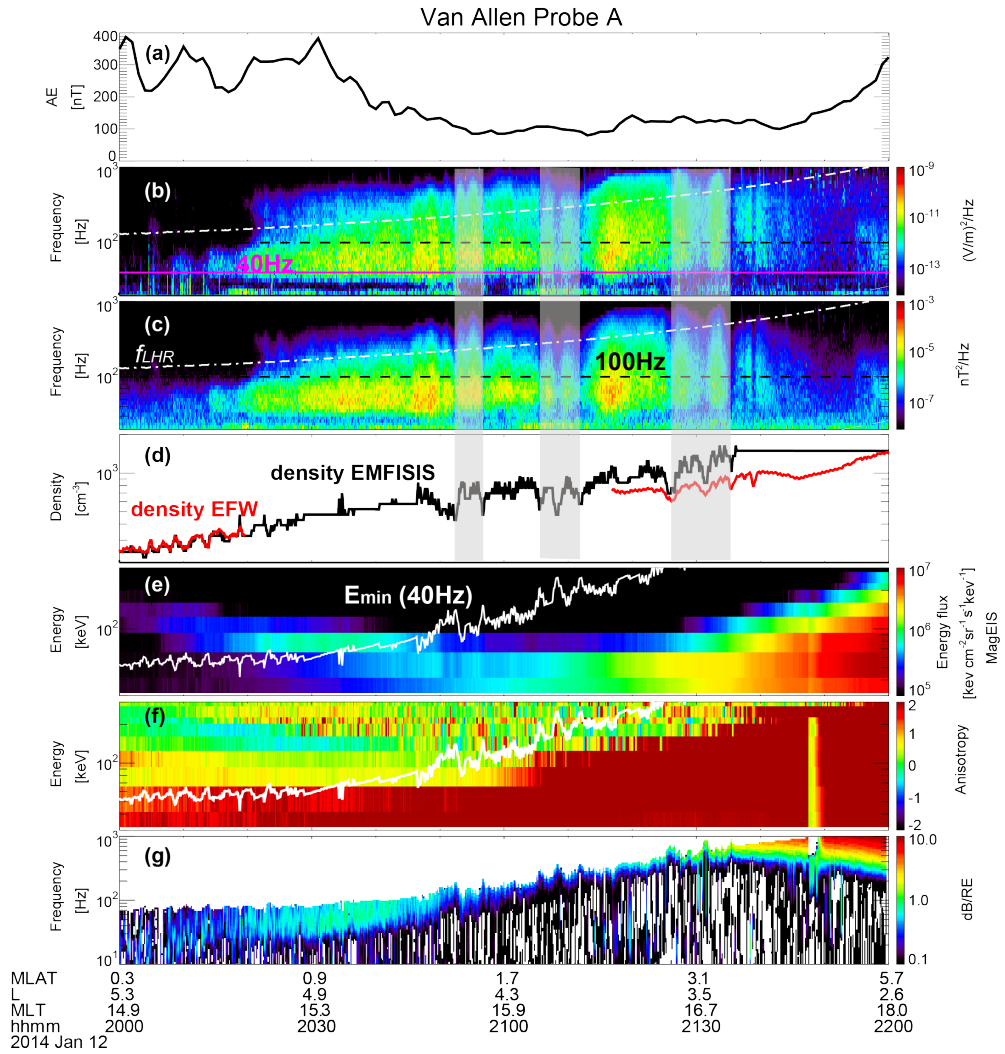
499



500 Figure 5



504 Figure 6

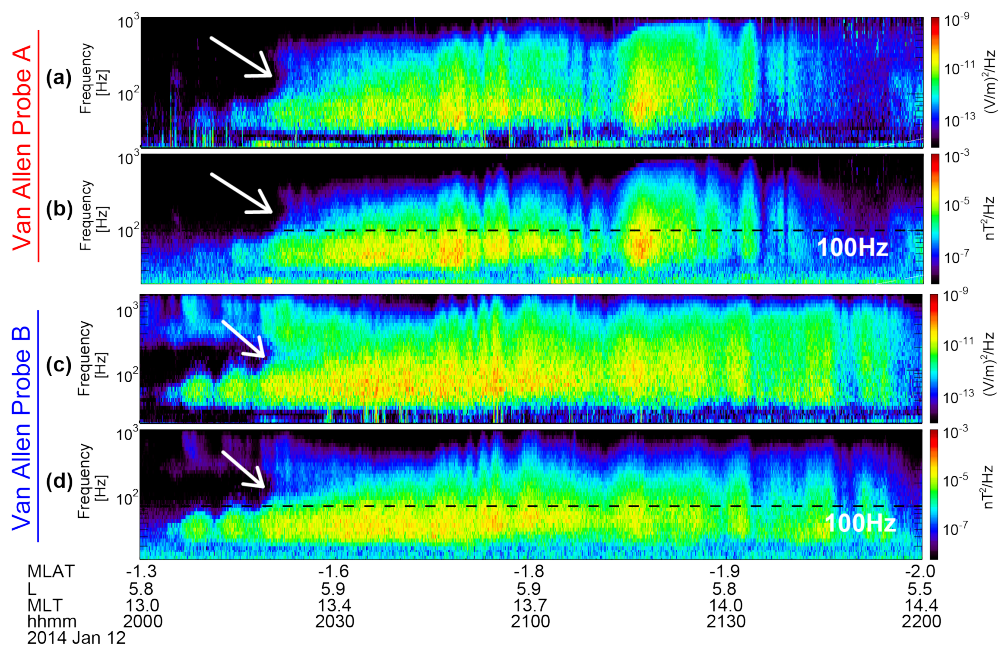


505

506



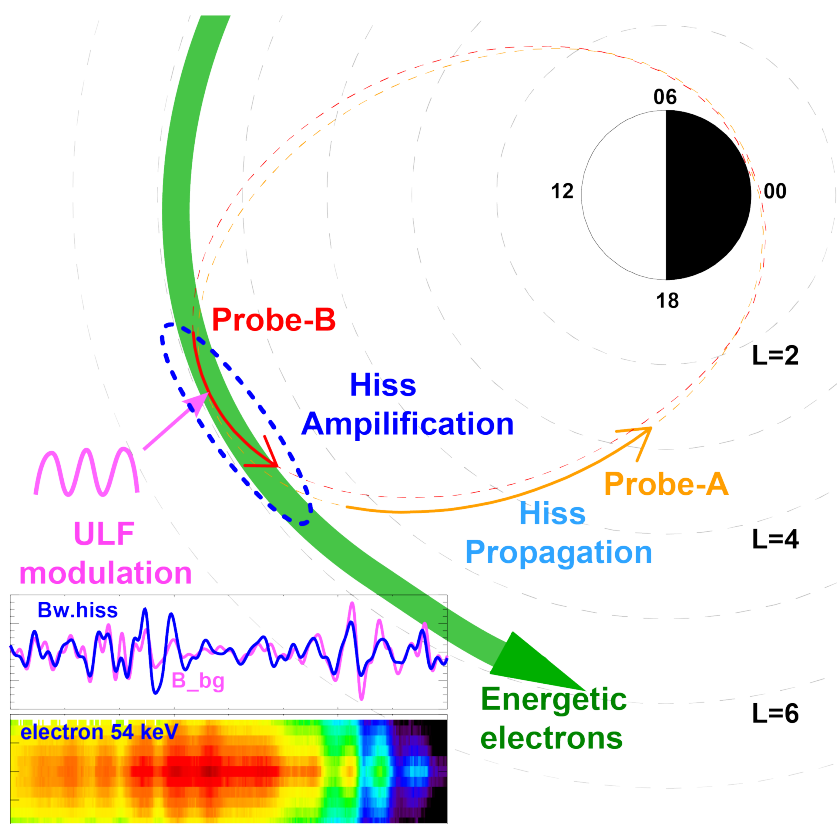
507 Figure 7



508  
 509



510 Figure 8



511